Applied Physics A (2019) 125:293
https://doi.org/10.1007/s00339-019-2592-y

Applied Physics A
Materials Science & Processing

Planar Hall effect and anisotropic magnetoresistance in semiconducting and conducting oxide thin films

Christer R. Akouala[1] · Raj Kumar[1] · Sandhyarani Punugupati[1] · C. Lewis Reynolds Jr.[1] · Judith G. Reynolds[1,2] · Edward J. Mily[1] · Jon-Paul Maria[1] · Jagdish Narayan[1] · Frank Hunte[1]

Received: 7 October 2018 / Accepted: 27 March 2019 / Published online: 3 April 2019

Abstract
Transport measurement techniques are generally considered to be indirect methods of probing the phenomenology of materials and hence are limited in scope and require careful interpretation. However, when performed with due care and precision in addition to other characterization methods, magnetotransport measurements are an essential tool in the study of magnetic and electronic materials particularly in proving potential devices that function on the basis of charge or spin transport. In this work, we demonstrate the advantage of employing a method that simultaneously measures the planar Hall effect and the anisotropic magnetoresistance which are two aspects of the resistivity anisotropy to characterize a range of semiconducting and conducting oxide thin films. The development of novel magnetotransport characterization methods is motivated by the need for reliable measurements of the electronic properties of a wide range of materials under varying thermal, mechanical and magnetic conditions.

1 Introduction

Magnetic semiconductors that exhibit robust ferromagnetism at or above room temperature can be useful materials for the development of spintronic devices, i.e., devices that function by utilizing both the charge and spin characteristics of conduction electrons for the transmission and storage of information [1, 2]. The major challenges that have inhibited development of spintronic devices include the availability of materials with Curie temperature ≥ 300 K in addition to the ability to distinguish between their intrinsic magnetic properties and extrinsic (contamination induced) magnetism [2, 3]. Magnetotransport methods are valuable techniques for characterizing thin film materials that are magnetic semiconductors [4, 5]. Since magnetometry only gives results from the bulk of the sample (including sub-layers, i.e., substrates and buffer layers), it becomes increasingly difficult to discern whether the magnetization is due to the thin film only or whether it is due to the sub-layers or environmental doping. Magnetotransport techniques are important because they provide a method of studying spin-dependent charge transport, whether in-plane or out-of-plane of the sample of interest.

Commonly utilized techniques such as the Hall effect and magnetoresistance can be used to measure the charge transport within a thin film when a magnetic field is applied perpendicular and out of the plane of the film. These techniques are useful, as evidenced by their extensive use in the semiconductor industry, for determining the majority carrier type, concentration, and mobility. The simultaneous measurement of the planar Hall effect (PHE) and anisotropic magnetoresistance (AMR) measurements are complementary to the typical perpendicular field techniques and magnetometry. The usefulness of PHE and AMR stems from the fact that they are only dependent on spin order-induced scattering; this means that these measurements are solely due to the interaction between magnetization (spin ordering) and charge transport. PHE and AMR are phenomena in which the magnetic field mainly serves to align the magnetization within the plane of the film. With this arrangement, it is then possible to study the angular dependence (anisotropy) of the magnetization, which is separate from simply determining whether a semiconductor is ferromagnetic. This phenomenon can be useful in the design of magnetoresistive sensors, especially

✉ Christer R. Akouala
akoualacr@appstate.edu

[1] Department of Materials Science and Engineering, North Carolina State University, Raleigh, NC 27695, USA

[2] Department of Physics, North Carolina State University, Raleigh, NC 27695, USA

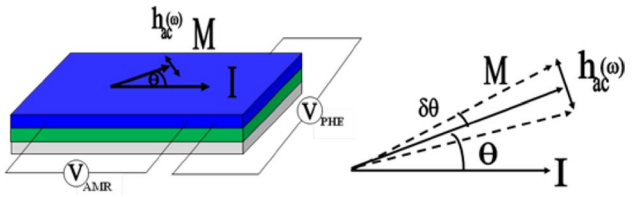

Fig. 1 (Left) Configuration for AMR and PHE measurement of thin film bilayers of FM-AF with magnetization relative to the current direction and (right) small changes in angular orientation of magnetization relative to the direction of current

as read heads for magnetic storage media. For these sensors to become useful, the giant planar Hall effect (GPHE) must be demonstrated at room temperature.

A variation of this method by way of the simultaneous measurement of ac-AMR and ac-PHE was used to probe the exchange coupling between a ferromagnet and an antiferromagnetic layer as shown in Fig. 1. This technique is similar to the ac-susceptometry of Strom et al. [6, 7].

An additional advantage of the simultaneous measurement of the ac-AMR and ac-PHE is that the magnetization can be probed with enhanced sensitivity, independent of the angle between magnetization and current direction. When sensitivity to the response signal is diminished in one aspect of the resistivity anisotropy at some angle of orientation, it is enhanced in the other over a full angular range of 360°. Figure 2 shows graphs of the AMR and PHE data for a thin layer of Co deposited on a CoO substrate by dc magnetron sputtering measured at 410 Hz, the frequency of the excitation current for the resistance measurement [8–10]. It can be seen that when sensitivity ($\Delta R/\Delta\Theta$) to changes in resistance with small angular oscillations of the magnetization due to a small ac magnetic field ($h_{ac}(\omega)$ in Fig. 2 [11]) is lost in the AMR, the response can still be detected with the PHE. Likewise, when sensitivity in the PHE is diminished, sensitivity is enhanced with the AMR signal. In this way, magnetization reversal, rotation and dispersion of easy axes can be probed with high precision.

By applying a small ac magnetic field ($h_{ac}(\omega) \sim 5$ Oe) perpendicular to the dc field, the "*derivatives*" (the ac-AMR and ac-PHE) of the AMR and PHE are obtained similar to a susceptibility measurement as:

$$\chi = \frac{dM}{dH} = \frac{dM}{d\theta} \cdot \frac{d\theta}{dt} \cdot \frac{dt}{dH} = \frac{(dM/dt)}{(dH/dt)} \quad (1)$$

The response of the magnetization is detected at the fundamental frequency of the ac magnetic field. In an AMR measurement, other harmonics appear because of the frequency of the excitation current for the resistance measurement. This combination of magnetic fields allows

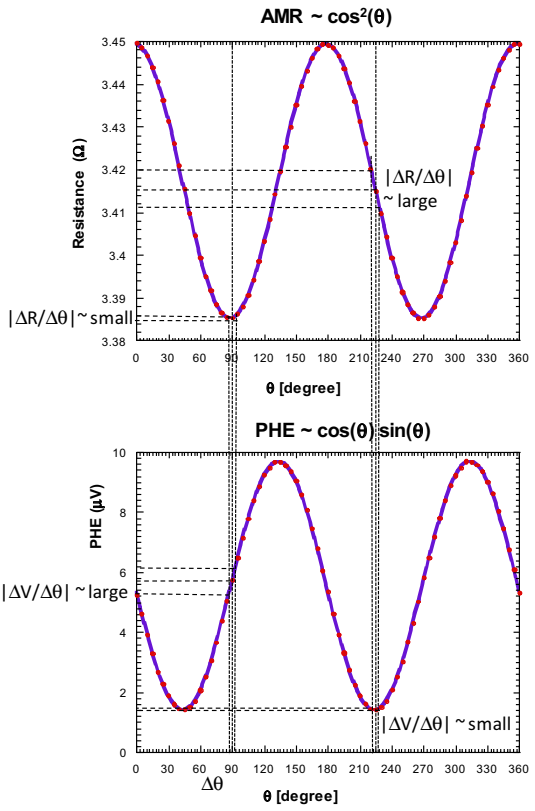

Fig. 2 Angular variation of resistivity anisotropy. **a** AMR and **b** PHE with applied magnetic field in exchange coupled Co/CoO bilayers

the magnetization in the sample to be probed over the entire magnetization curve M versus H. Small changes can be detected, since the ac measurement is sensitive to the slope of the magnetization curve. Both the real and imaginary parts of the magnetization response are measured similar to the ac susceptibility. The real (in-phase) part corresponds to the stiffness of the exchange coupling, while the imaginary (out-of-phase) part corresponds to the dissipation.

General galvanomagnetic effects appear even in nonmagnetic materials due to the presence of electric fields, magnetic fields and temperature gradients. However, there are two contributions to these effects in ferromagnetic materials: (1) the presence of the spontaneous magnetization and (2) the applied field. In ferromagnetic conductors, the magnetoresistance is anisotropic due to the asymmetric scattering of conduction electrons [12]. The planar Hall effect (PHE) is the transversal manifestation of this planar resistivity anisotropy. PHE is a misnomer since its origin is different from the normal Hall effect. The conventional Hall effect is due to the Lorentz force on conduction electrons which generates a transverse (Hall) voltage across a conducting material and normal to the applied magnetic field. The origin of the PHE is attributed to the interaction between the magnetization

and current in the plane of the film. Consequently, the resistivity in magnetic conductors is very dependent on the direction of the magnetization with respect to the current flow. In fact, the anisotropic magnetoresistance (AMR) and the planar Hall effect can be described as the longitudinal and transverse components of the anisotropic resistivity [13]. They are described by their characteristic dependence on the angle between magnetization and current (as shown in Fig. 1), which can be described by the equations below for the AMR and PHE resistivities.

$$\rho_{\mathrm{AMR}} = \rho_{\perp} + (\Delta\rho)\cos^2\theta \tag{2}$$

$$\rho_{\mathrm{PHE}} = (\Delta\rho)\sin\theta\cos\theta = \frac{(\Delta\rho)}{2}\sin 2\theta \tag{3}$$

$$\Delta\rho = \rho_{\parallel} - \rho_{\perp} \tag{4}$$

For the current parallel to the magnetization, resistivity has a value of $\rho_{//}$ and $\rho_{\perp}$ for the perpendicular case.

Both PHE and AMR have their origins in the dependence of the resistivity on the orientation of the magnetization [14, 15]. Spin-dependent transport then gives rise to different scattering when changing the angle between the magnetization and electric current directions. Although the exact parameters underlying anisotropic magnetoresistance are not yet fully understood, three microscopic theories [16, 17] have contributed to further understanding the resistivity anisotropy in ferromagnetic materials: (1) Mott's two-current model, (2) Smit's addition of spin–orbit coupling and (3) Potter's model with exchange splitting of energy bands. These models are summarized below.

Mott considered a model in which two independent channels of 4s electrons, spin up (majority) and spin down (minority) in ferromagnets, were responsible for the electrical conduction with negligible contribution from 3d electrons due to their large effective mass [16, 17]. According to this model, the conduction electrons undergo s–s or s–d transitions during which their spins remain unchanged and the spin exchange between s electrons is ignored. More frequent s–d transitions correspond to higher scattering, and thus, higher resistivity. This model explained the high resistivity and negative magnetoresistance of ferromagnetic metals such as Ni [16, 17]. Unfortunately, Mott's assumption of spherical and parabolic, i.e., isotropic, bands leads to this model's failure to explain anisotropic effects. The assumption of isotropic bands leads to an expected isotropic resistivity, which is certainly not the case. This shortcoming was tackled by Smit's suggestion of a spin–orbit coupling contribution.

If s–d interband scattering is the dominant feature of transition metal electronic conductivity, then the resistivity anisotropy in ferromagnetic conductors must be due to an anisotropic scattering mechanism. Smit, therefore, proposed that an isotropic scattering potential with lower-than-cubic-symmetry-wave functions due to spin–orbit interaction could be responsible for the resistivity anisotropy in ferromagnets [16, 17]. Spin–orbit interaction also makes a magnetization, i.e., spin, direction-dependent contribution to the energy of the d states. This explains the magnetocrystalline anisotropy, which means that the magnetization direction is more favorable in certain crystallographic directions. Therefore, the d electron spin is coupled to its orbital motion, which is then coupled to the lattice by the crystalline field. The spin–orbit interaction ($H_{\mathrm{spin-orbit}} = KL \bullet S$; K is the spin–orbit coupling parameter) is treated as a small perturbation which results in a mix of states with parallel and antiparallel spins. Unoccupied parallel d states are always present, but these holes are unequally distributed over the five possible d orbits; there is, however, a deficiency of hole orbits when electrons move perpendicular to the magnetization. The transition of an s electron to a d state under the influence of a perturbing potential is less likely if the s electrons moves perpendicular to the plane of the orbit (i.e., parallel to the magnetization since there are few hole orbits in this direction). Therefore, it follows that the s electrons are more easily trapped when moving parallel to the magnetization rather than in a perpendicular direction. This leads to the expected conclusion that in ferromagnetic conductors, the anisotropy constant $\Delta\rho$ is positive, i.e., $\rho_{//} > \rho_{\perp}$.

Another model, proposed by Potter suggested that $\Delta\rho$ could be either positive or negative depending on whether the anisotropy was due to minority-spin electrons (as in Smit's case) or majority-spin electrons, respectively [16, 17]. The major difference with Smit's model is that Potter's model assumed that the d bands were uniformly exchange split with some energy separations. Potter's model is very useful because it suggests that the ratio of K, the spin–orbit coupling parameter, to the splitting energy of the two uppermost d bands is important to produce a large anisotropy constant. This then would be useful in determining which materials would likely lead to PHE/AMR signatures at room temperature with potential applications in next generation devices.

The planar Hall effect is a phenomenon that can be used for characterizing magnetic semiconductors and has the potential to provide insight into the mechanism for magnetic behavior in magnetic conducting oxide thin films that are undoped. In addition, its observation would be a clear indication that there exists a definite ferromagnetic ordering within the undoped magnetic conducting oxide investigated herein. This phenomenon has been used in the study of exchange coupling between magnetic multilayers, such as NiFe/NiMn [18] and Co/Cu films [19]. Additionally, it has been used in the study of thin films of Ga(Mn)As [20], LSMO [13] and Permalloy [21]. PHE has also been studied for low-field magnetic sensor applications [22]. In all cases

where the planar Hall effect was used to characterize thin films, it proved to be a powerful tool for studying the in-plane magnetization reversal processes because of its high sensitivity to the direction of magnetization.

Here we report the observation of the PHE and AMR at various temperatures (including room temperature) in ZnO and CuO, two oxide materials with varying electrical and magnetic properties. We emphasize that this investigation of the planar Hall effect and anisotropic magnetoresistance is separate from the simple observation of ferromagnetism in these metal oxide thin films. While one might consider investigation of the planar Hall effect and anisotropic magnetoresistance in the strongly magnetic hexaferrites and manganites (see, for example, references [23–27] by Trukhanov, et al.), our focus was based on spintronic applications of dilute magnetic semiconductors in which carrier transport is dominated by electrons and holes in ZnO and CuO, respectively. Further, demonstration of PHE and AMR in these materials shows the sensitivity of these techniques for elucidating the nature of spin-dependent transport even in weakly magnetic systems.

1.1 Sample preparation

The ZnO thin films were epitaxially grown on single crystal c-plane sapphire substrates by two techniques, pulsed laser deposition (PLD) and metal-organic vapor phase epitaxy (MOVPE). For the PLD deposition, a KrF excimer laser ($\lambda = 248$ nm, pulse duration = 25 ns) with a pulse energy density of 2.8 J/cm^2 at a repetition rate of 10 Hz was used. The target–substrate distance was maintained at 4 cm during the film deposition. A high-purity ZnO target was prepared using a solid-state reaction technique. Special care was taken to avoid any transition metal contamination, e.g., nonmagnetic plastic tweezers were used throughout the sample growth and characterization processes. Before deposition, the sapphire substrate went through a surface cleaning procedure which involved sonicating in acetone, methanol, and DI water, each for 5 min. The sample was deposited at room temperature (300 K) with an oxygen partial pressure of 10^{-3} Torr, which resulted in a PLD film that was 500 nm thick. The deposition chamber was evacuated to a base pressure of less than 10^{-6} Torr before the introduction of oxygen. The MOVPE sample was grown in a vertical reactor at a pressure of 50 Torr in the temperature range 480–490 °C with N_2 as the carrier gas. Diethylzinc (DEZ) and nitrous oxide (N_2O) are used as the precursors. In addition, 3% nitric oxide (NO) in N_2 provides ions in the + 2 oxidation state for doping if desired. By alternating between steps of low Zn partial pressure and high Zn partial pressure, the formation of Zn vacancies and O vacancies was induced, respectively. The energetics of these reactions favors the formation of V_O–N_{Zn} pairs, which are double donors. These two steps were repeated until the desired thickness (600 nm) is reached. Further details on the MOVPE growth are discussed elsewhere [28]. The crystal structure of these films was characterized by X-ray diffraction (XRD) using a Rigaku X-ray diffractometer with Cu Kα radiation ($\lambda = 0.154$ nm). The relevance of the nominally undoped ZnO thin films grown by two different techniques is that the growth mechanisms are quite different. While MOVPE is considered a near-equilibrium technique, PLD is highly non-equilibrium, which has the potential to give rise to different defect chemistries. Hence, the observation of the PHE and AMR in these films suggests that their presence is intrinsic to ZnO. The p-type CuO thin films were grown on Si substrates in a magnetron sputtering chamber.

1.2 Measurement techniques

Measurements of the resistivity variation with temperature over a range from 300 to 5 K were conducted in the Van der Pauw geometry in a Quantum Design 9T Physical Property Measurement System (PPMS) with base temperature ~ 2 K. Hall effect measurements were also performed in the PPMS using the same geometry. The van der Pauw configuration was used for Hall effect measurements at room temperature and for MR at all temperatures. Samples were approximately square with 0.5–1 cm sides. From Hall effect (transverse voltage) measurements, the majority carrier type, concentration and mobility were determined. From longitudinal voltage measurements, the magnetoresistance, i.e., degree of spin ordering, could be calculated, and resistivity vs. temperature can be acquired.

Magnetometry was carried out using a superconducting quantum interference device vibrating sample magnetometer (SQUID-VSM, Quantum Design). The 2 mm by 2 mm samples were mounted on a quartz holder using GE 7031-varnish and dried. The dried sample was then loaded into the SQUID-MPMS. The magnetic moment vs. field and temperature were then acquired. The magnetic moment (emu) was normalized to magnetization (emu-cm^{-3}) using the volume of each sample. Sample volume was determined by multiplying the film thickness by the sample area.

Some PHE measurements were conducted on a custom-built setup for AMR-PHE characterization consisting of a cryostat attached to a GMW 3T electromagnet. Most of AMR-PHE measurements, however, were performed in the PPMS. In all transport measurements, including PHE, ohmic contacts with the sample surface were made using gold-plated pogo pins. dc magnetron sputtering was used to deposit gold contacts on the MOVPE samples. For PHE measurements, a constant in-plane magnetic field was applied while the orientation of the applied current (i.e., the sample) was rotated counterclockwise.

The same 0.5–1 cm samples were used for PHE and AMR measurements. The sample was mounted parallel to

the magnetic field direction. The sample surface defines the rotation plane for the angle between magnetization (and magnetic field) and the current. The magnetic field is maintained at a constant value to provide sufficient magnetization to the sample and hence a clearer signal for the angular dependence of PHE and AMR. During the experiment, the current direction in the sample is rotated from 0° to 360°, while the PHE and AMR signals are simultaneously recorded. PHE and AMR are first measured at different fields from 0, 0.5, 1, 3, 5, 7, and 9 T to find the field at which the highest signal is generated (7.5T), and then they are measured at that magnetic field at temperatures from 5 to 300 K.

2 Results and discussion

2.1 PHE/AMR in ZnO

Figure 3 shows the θ–2θ scans of the XRD measurements for ZnO thin films grown on c-plane sapphire by MOVPE and PLD. For the MOVPE grown sample, the θ–2θ scan reveals only (002) and (004) reflections, which is indicative of highly c-axis oriented thin films with good quality. The PLD sample showed only a very weak intensity (002) peak, which suggests that the sample is nanocrystalline and/or highly textured. Within the detection limits of the XRD system, no secondary magnetic phases are present in the X-ray diffraction patterns.

Figure 4 shows the variation of resistivity with temperature, which clearly shows characteristic semiconducting behavior expected for ZnO thin films. Although the X-ray data of the PLD-grown sample suggested a nanocrystalline or highly textured film, this sample exhibited an overall lower resistivity than the MOVPE grown sample over the entire temperature range from 5 to 300 K. Most likely, the lower resistivity in the PLD sample is related to a higher oxygen vacancy concentration, as discussed by Mal, et al. and below. Furthermore, the resistivity of both samples grown by PLD showed a well-defined exponential behavior which is consistent with simple thermal activation of charge carriers from an unintentional donor level within the band gap to the conduction band.

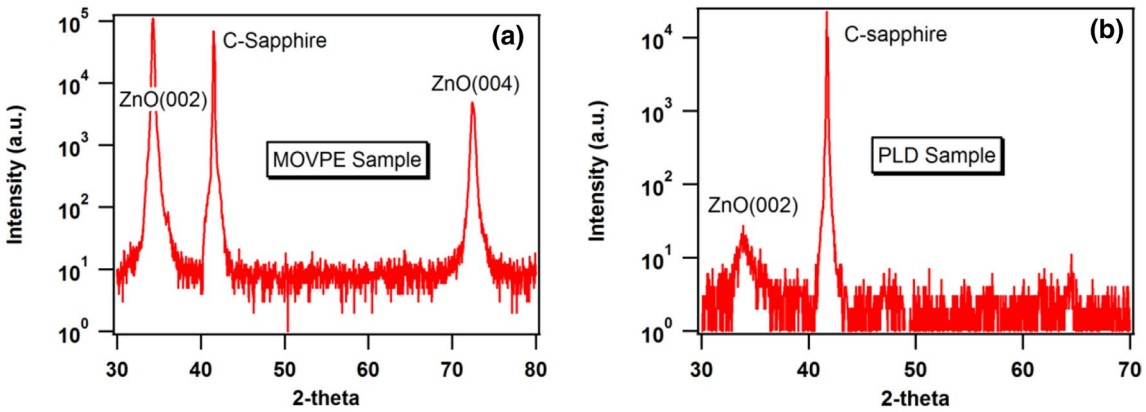

Fig. 3 X-ray diffraction θ–2θ scans of **a** MOVPE and **b** PLD-grown ZnO thin films

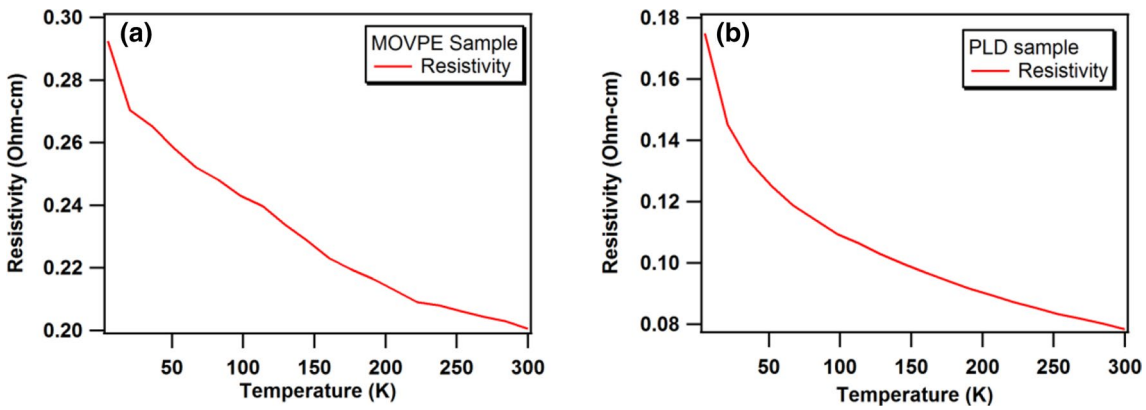

Fig. 4 Resistivity vs. temperature of **a** MOVPE, and **b** PLD ZnO thin films

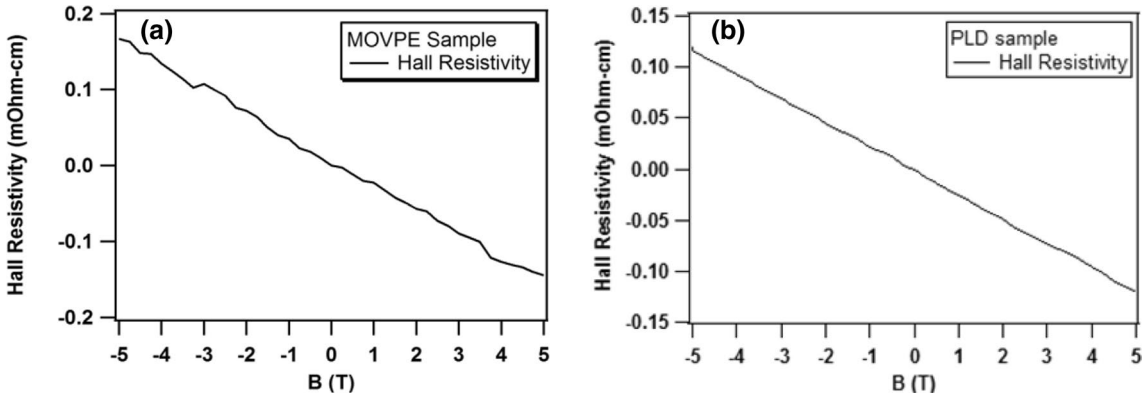

Fig. 5 Hall resistivity vs. applied magnetic field for **a** MOVPE and **b** PLD-grown undoped ZnO thin films

The change in Hall resistivity with applied magnetic field is shown in Fig. 5, in which the negative slope observed for both samples is indicative of n-type semiconducting behavior. In addition, estimates of the carrier concentration from these data at 300 K yielded 2×10^{18} cm^{-3} for the MOVPE ZnO and 7×10^{19} cm^{-3} for the PLD ZnO. Since these samples are nominally undoped, this high carrier concentration is most likely an indirect indication of a high level of native defects, which have implications for the magnetic properties, as discussed below. The combination of temperature dependence of resistivity and the magnetic field dependence of the Hall resistivity indicate that both films are n-type semiconductors. In terms of band structure and band filling, stoichiometric ZnO is a wide-bandgap semiconductor or might be considered an insulator, since the two 4s electrons in Zn are transferred to the oxygen 2p band, making the valence band completely full. If, however, oxygen vacancies or Zn interstitials are introduced into the crystal lattice through annealing in a reducing atmosphere (causing neutral oxygen to leave the crystal), then the valence electrons of these oxygen vacancies or zinc interstitials can be easily excited and act as donors [29]. Furthermore, charge neutrality requires that there be a maximum of two electrons along with the oxygen vacancies in the place of the missing oxygen atoms. Consequently, then, in non-stoichiometric ZnO, we have a defect structure that has an oxygen vacancy with electrons from the conduction band localized on adjacent zinc sites in the form of Zn^{+} ions [30]. Therefore, non-stoichiometric ZnO is an n-type semiconductor [29]. Since our nominally undoped samples are all n-type, it is likely that they are non-stoichiometric and contain lattice defects.

The magnetic field dependence of the magnetization of both samples showed hysteretic behavior with the saturation field occurring near 1000 Oe for the MOVPE sample (Fig. 6a), and 5000 Oe for the PLD-grown sample (Fig. 6b). The PLD sample shows a saturation magnetization of 4.4 emu-cm^{-3} at room temperature with a slight increase with decreasing temperature. The MOVPE shows a saturation magnetization of 0.4 emu-cm^{-3}at room temperature with a slight increase to ~ 1 emu-cm^{-3} at the lowest temperature. The higher saturation field in the PLD sample most likely suggests that this sample has a higher concentration

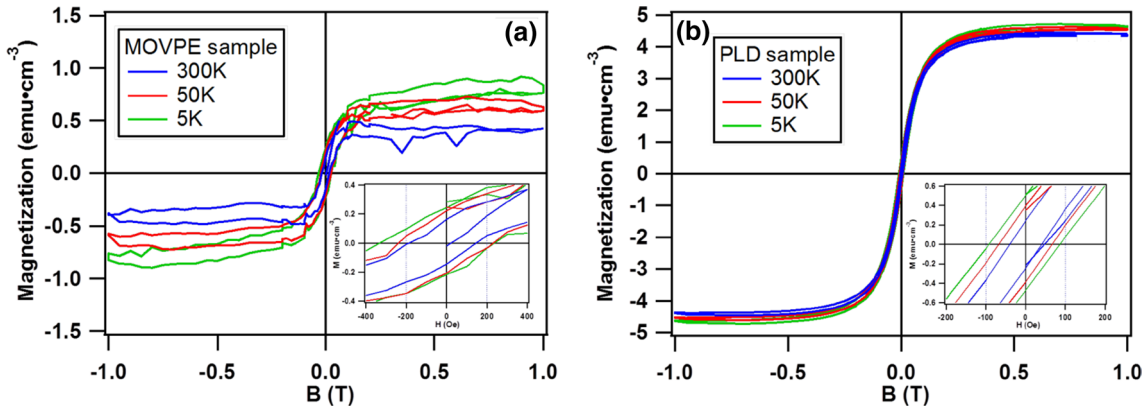

Fig. 6 Magnetization vs. applied field for **a** MOVPE, and **b** PLD ZnO

of O vacancies resulting in defect-mediated ferromagnetic behavior. Both samples have clear coercivity widths that expand with decreasing temperature as can be seen in the insets of Fig. 6. Coercivity is considered the resistance of a ferromagnetic material to becoming demagnetized. There is an expected increase in magnetic ordering as the temperature decreases since thermal fluctuation effects are decreased. This increased ordering is most likely why the coercivity increases at lower temperatures, meaning that the magnetic ordering makes the sample more resistive to demagnetization. Since these samples are both nominally undoped, one must explore other sources for the magnetic behavior, since X-ray diffraction did not reveal the presence of any secondary magnetic phases. We postulate that the origin of the magnetic behavior in these samples lies in the intrinsic defect structure of these ZnO thin films, specifically oxygen vacancies. Mal et al. previously showed that oxygen vacancies play a key role in the magnetic properties of ZnO [31]. They demonstrated that one could tune the ferromagnetic behavior in ZnO films by varying the oxygen vacancy content through various annealing steps. Ferromagnetic behavior was enhanced through an increase in oxygen vacancies by thermal annealing and/or laser irradiation [32] or suppressed, that is, becomes diamagnetic by annealing in an oxygen environment [31, 32]. The lower saturation magnetization and lower carrier concentration in the MOVPE sample are consistent with this.

This phenomenon of magnetic behavior in materials that contain no magnetic ions has been called d^0 ferromagnetism [8], since the atoms contain no unpaired d-electron spins. This contrasts with the localized magnetism theory which attributes ferromagnetism to unpaired electron spins in d-orbitals. Such d^0 ferromagnetism has been observed in irradiated graphite and hexaborides such as CaB_6 and HfO_2 [33]. Likewise, we suggest that the lattice defects in our ZnO thin films are the source of ferromagnetism. The defect structure (oxygen vacancies and Zn^+ ions) mentioned above in our discussion of electronic properties provides a source of electrons to the conduction band. Moreover, electrons can be trapped at the effective positive charge on the vacancy itself [34], forming what are called F and F^+ color centers. The difference between the two is that the F-center is comprised of a neutral oxygen vacancy with two trapped electrons, whereas the F^+ is a singly charged oxygen vacancy with only one trapped electron [35]. F and F^+ centers are known to form in MgO [27]. One should also note that defects have also been invoked to explain the observation of room temperature ferromagnetism in MgO [36]. Mackrodt [30] states that the association energy of a localized electron to a doubly charged oxygen vacancy is small (0.2 eV) leading the defect structure of reduced ZnO to contain singly and doubly charged oxygen vacancies along with F^+ centers, a complex (F^+–Zn_{Zn}) and conduction band electrons. Zn_{Zn} represents a Zn^{2+} ion on a normal cation site. Here we suggest that oxygen vacancies can serve as both a source of conduction electrons as well as a localized F/F^+ center for electrons. The F^+ center, which consists of a single electron trapped at the oxygen vacancy, exhibits paramagnetic behavior, which can be studied by electron paramagnetic resonance (EPR) [37, 38]. In reduced ZnO, then there is an interaction between localized (F^+ center) spin-polarized electrons and conduction electrons which may lead to carrier-mediated ferromagnetism. Mal et al. [32] attributed the ferromagnetic behavior in their undoped ZnO thin films as being due to polarization of trapped electrons by positively charged oxygen vacancy sites. Similarly, Gao et al. [39] used an "F-center exchange" mechanism to explain the origin of room temperature ferromagnetism in ZnO_2 nanoparticles. They explained that electrons trapped in singly charged oxygen vacancies (F^+) are strongly localized, and once the F^+ center density reaches a critical value for magnetic percolation, these centers overlap resulting in long-range ferromagnetic ordering even in the absence of itinerant carriers.

Recently, Choudhury proposed an F-center-mediated bound magnetic polaron to explain ferromagnetic behavior in Mn-doped TiO_2 nanoparticles [40]. In their model, they suggest that the ferromagnetic ordering is due to the interaction of neighboring Mn^{2+} ions via an oxygen vacancy (F^+ center). Since our samples are magnetically undoped, we propose instead that the oxygen vacancy itself is the source of the magnetic moment with the conduction electrons acting as the mediators of the interaction between neighboring oxygen vacancies. This is like the carrier-mediated ferromagnetism known as the bound magnetic polaron, in which oxygen vacancies act as both electron donors and electron traps. The trapped electrons couple the local moments in the host lattice within their orbit ferromagnetically leading to a large net magnetic moment [12]. Since the ZnO thin films investigated here exhibit both magnetic and semiconducting properties, it was anticipated that the planar Hall effect phenomenon would be observed. Measurements were performed to investigate this interaction between magnetization and the current flow direction in our samples. The angular dependence of the PHE is given in Eq. (2) and predicts extrema at angles of 45°, 135°, 225° and 315°. As shown in Fig. 7, these are exactly the angles at which we observe extrema in our nominally undoped films. The acquired data were fitted to a $\sin 2\theta$ curve displayed by the red line in Fig. 7. The PHE and AMR signals between samples can be compared using the resistivity constant $d\rho = \rho_{//} - \rho_{\perp}$. This constant is the difference between the resistivity parallel (0°) and perpendicular (90°) to the magnetization. The resistivity constant for the MOVPE sample as measured from the PHE experimental fits (red line in Fig. 7) is − 0.24 ohms, whereas it is − 0.30 ohms from our AMR fit (blue lines in Fig. 8). For

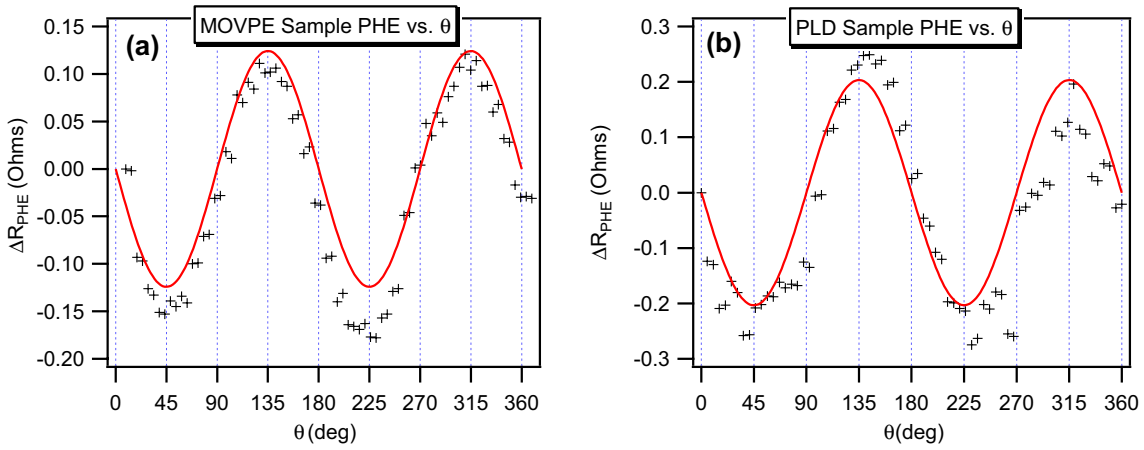

Fig. 7 PHE vs. angle at 4.2 K and 1T, for **a** MOVPE, and **b** PLD ZnO films

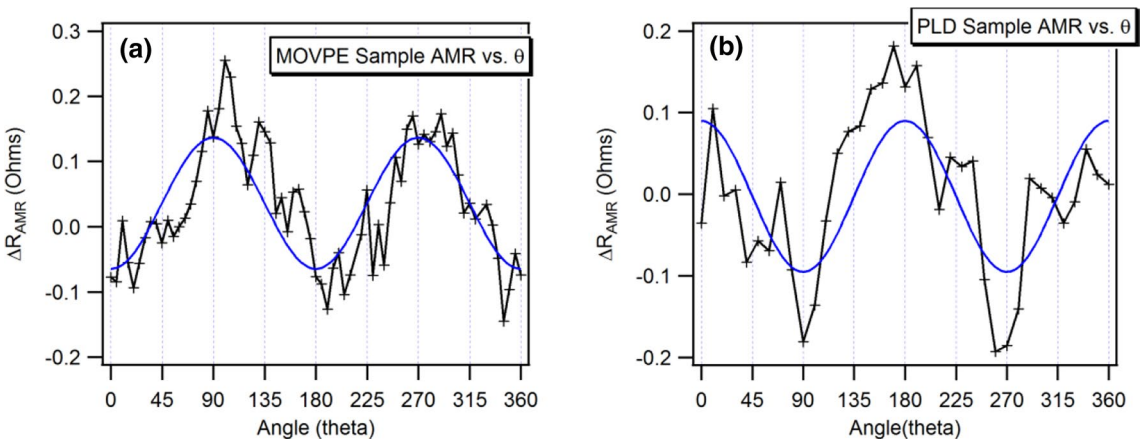

Fig. 8 AMR vs. angle at 4.2 K and 1T, for **a** MOVPE, and **b** PLD ZnO thin films

the PLD sample, the values are − 0.41 and − 0.30 ohms from PHE and AMR fits, respectively. For each sample, the same value was expected from the experimental fits to the PHE and AMR equations. However, the values are in the same order of magnitude with some deviation. Equations (1) and (2) assume a uniform current, while these films could be inhomogeneous, and the role of crystal anisotropy is yet to be studied. Nevertheless, one can see that the values are comparable.

The planar Hall effect should only be observed in magnetic conductors, since it depends on the orientation of magnetization in relation to the current flow direction. Our samples are magnetically undoped, yet they exhibit magnetic properties which we attribute to magnetic moments of electrons trapped within F-centers. Although there have been numerous reports of ferromagnetism in undoped ZnO [31, 32, 41–45], we must emphasize that this investigation is the first to report the planar Hall effect in ZnO. We have also measured the anisotropic magnetoresistance on the same samples as discussed below. The PHE is a sensitive technique for the characterization of intrinsic magnetism in magnetic semiconductors, since it depends only on the interaction between carriers and magnetization. It also provides us with insight into the mechanism for the magnetic behavior in ZnO thin films and clearly indicates the existence of definite magnetic ordering present within our samples. Both of our ZnO samples grown by quite different techniques exhibited the characteristic angular dependence of the PHE and AMR at 4.2 K with a constant applied field of 1 Tesla, as shown in Figs. 7 and 8, respectively. Both sets of data are consistent with the expected sin2θ behavior for the PHE in Eq. (2) although the PLD sample may exhibit some deviation which could be associated with the nanocrystalline or the textured nature of this sample as suggested above by the XRD data and scattering mechanisms within the crystal. These results, however, strongly suggest that the magnetic order which we observe via the PHE is intrinsic to ZnO and its defect structure.

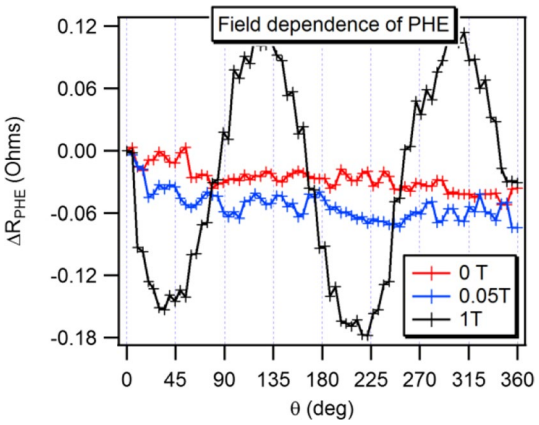

Fig. 9 PHE vs. angle at different magnetic field values for MOVPE grown ZnO

Figure 9 reveals that there is no visible sin2θ behavior at very low fields in the MOVPE sample; this suggests that there is randomization of the magnetic moments (that is, a lack of magnetic order) below the saturation field leading to an overall constant resistance even as the direction of current is rotated. An applied field of 1 Tesla, however, is sufficient to produce a saturation magnetization which results in the expected angular behavior of the planar Hall effect. This can be correlated to the M vs H behavior shown in Fig. 6, which showed that the magnetization of the MOVPE sample is saturated at ~ 1000 Oe (0.1 T). We expect that the PHE angular behavior should be visible at an applied field greater than or equal to this value.

2.2 PHE/AMR in CuO

Copper oxide (CuO) thin films on silicon substrates grown by magnetron sputtering were also investigated. The importance of these samples (50 nm thickness) is that they were p-type with high carrier concentration, 1×10^{21} cm^{-3}, at room temperature, whereas the ZnO samples were n-type. The Hall effect (Fig. 10a) was used to determine the majority carrier type. This high carrier concentration is usually characteristic of degenerate semiconductors. That is, a semiconductor with such a high carrier concentration that it begins to behave like a metal. The resistivity vs. temperature (Fig. 10b) confirmed this metallic conduction, but with the addition of a resistivity minimum around 100 K and a steady state at 34 K and below. There are two common explanations for the appearance of this resistivity minimum: electron–electron interactions and the Kondo effect. The Kondo effect is due to the strong coupling between conduction electrons and magnetic impurities at low temperatures. Kondo explained this behavior as being due to spin-flip scattering between the conduction electrons and the localized spin [46, 47]. The theory states that at low temperatures, each local spin becomes locked into a collective state (singlet) with the conduction band spins. At high temperatures, spin-flip occurs due to thermal energy, but as temperature decreases, the spin-flips become frozen and the Kondo effect saturates. Both the resistivity minimum and saturation are characteristic of the Kondo effect [46, 48].

As mentioned in the introduction, the electronic and magnetic properties have been correlated with the presence of small amounts of copper Cu^{3+} which increase the paramagnetic signal and give rise to conduction by holes in non-stoichiometric samples. XPS of CuO (Fig. 11) showed a main peak, Cu $2p_{3/2}$ with a binding energy of 933.4 ± 0.2 eV and a satellite peak ~ 9 eV greater than the main peak [49]. This satellite peak is reported to be characteristic of materials having a d^0 configuration in the ground state. The presence of copper in Cu^{2+} and Cu^{3+} states can lead to ferromagnetic interactions, as shown in Ref. [50].

The samples studied here showed soft ferromagnetic characteristics at room temperature, with a 1.5 emu-cm^{-3} saturation magnetization for sample 1. At 5 K, this saturation magnetization increased to 2 emu-cm^{-3} (Fig. 12a).

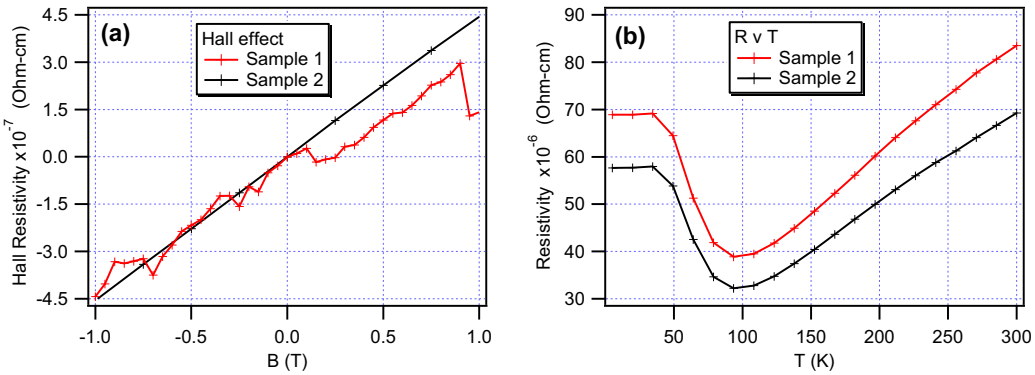

Fig. 10 **a** Hall effect and **b** resistivity vs. temperature for 50 nm CuO

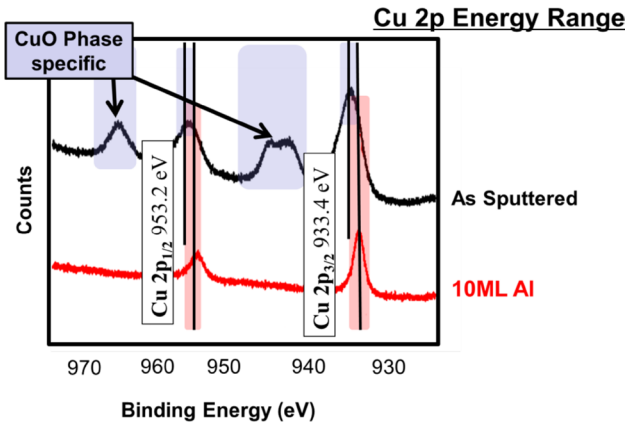

Fig. 11 Copper oxide phase confirmation, only the as-sputtered sample was used in PHE studies. XPS by Ed Mily is reproduced here with his permission

Room temperature saturation magnetization for sample 2 was 6.65 emu-cm^{-3} which did not change down to 5 K (Fig. 12b).

The theory of dilute magnetic semiconductors by Dietl predicted room temperature ferromagnetism in several material systems with Mn doping and hole concentrations > 10^{20} cm^{-3} [51]. This requirement in Dietl's model essentially demands a degenerate semiconductor, which is what we observed in the measured CuO samples, albeit without any magnetic doping. Measuring the planar Hall effect and anisotropic magnetoresistance at different temperatures showed the expected characteristic angular dependence for both samples (Figs. 13, 14). The PHE signature has never been previously reported in CuO at any temperature. It was observed that the maximum value for the PHE constant (which occurs at 100 K) is similar for the two samples (dρ ~ 2 Ohms). There is visible asymmetry in the AMR angular scans which is likely due to the monoclinic crystal structure of CuO. The role of crystal anisotropy on the PHE and AMR behavior is yet to be determined. Further work is needed to fully understand the PHE and AMR in CuO, but at this point it is conclusive that PHE/AMR are observed and are reproducible over the temperature range investigated in these p-type

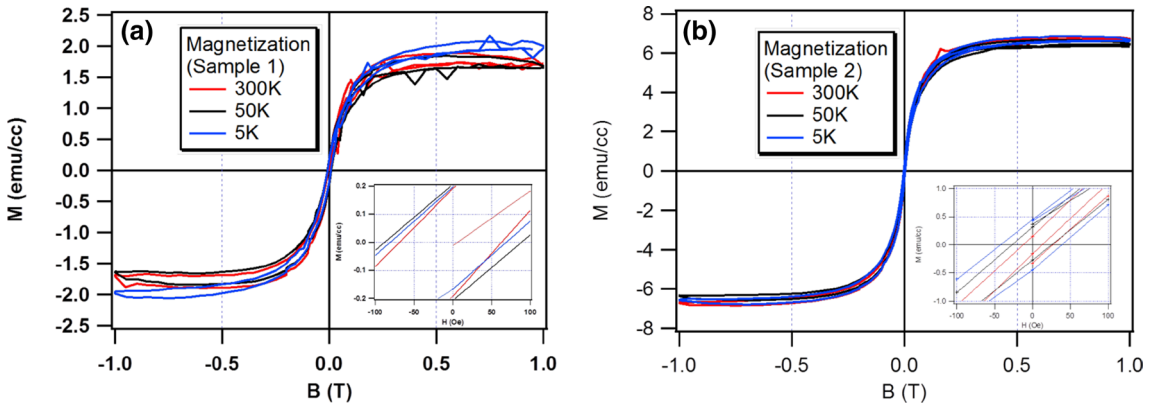

Fig. 12 Temperature dependence of magnetization vs. magnetic field for **a** sample 1 and **b** sample 2

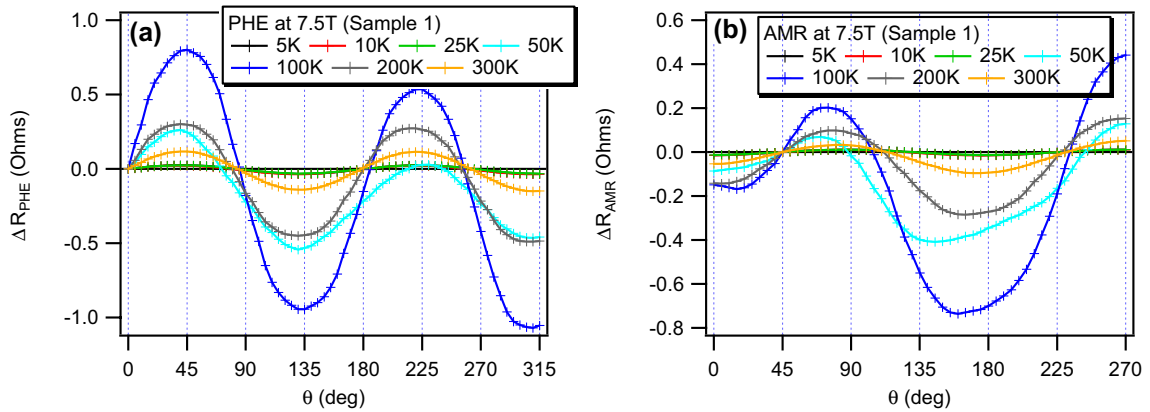

Fig. 13 Temperature dependence of **a** PHE vs. angle and **b** AMR vs. angle for sample 1

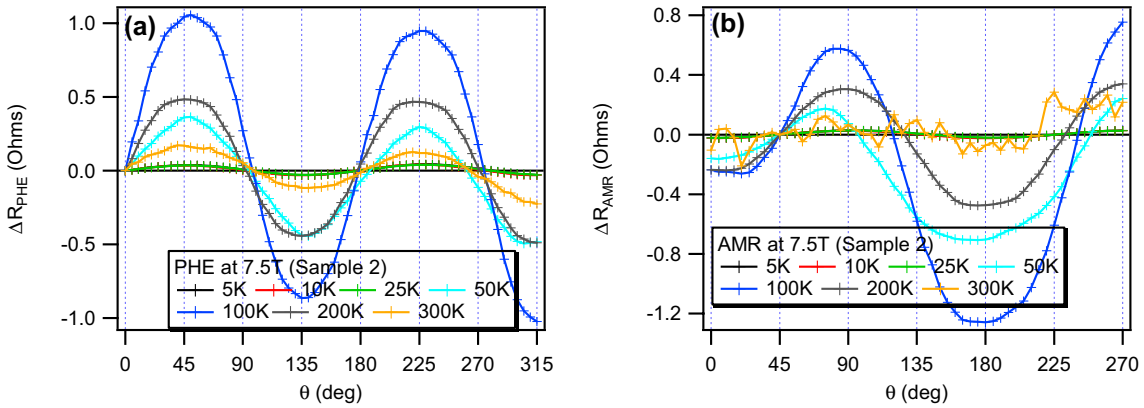

Fig. 14 Temperature dependence of **a** PHE and **b** AMR vs. angle for sample 2

degenerate semiconductors with soft FM and nanocrystalline structure.

3 Conclusions

The planar Hall effect was studied and displayed in thin films of defect-engineered magnetic conducting oxides ZnO and CuO. PHE and AMR were used as complimentary to magnetometry (bulk measurement) to ascertain the existence of charge and spin-dependent transport. Metal oxides, especially transition metal oxides, were chosen as the ideal system for the study of PHE because of the interesting changes in their magnetic and conducting properties due to their defect structures. Thin films of these samples are usually non-stoichiometric and the resulting lattice defects result in charge conducting behavior and different magnetic behaviors. ZnO has been shown to be n-type semiconductor and exhibit room temperature ferromagnetism when it is in small dimensions, for example, thin films, nanoparticles. On the other hand, CuO is a degenerate p-type conductor and is an antiferromagnet with differing behavior as temperature decreases.

The PHE was observed in undoped ZnO at the onset of 100 K, and the signal increased with decreased temperature. The sign of the PHE constant dρ was negative. The temperature dependence was also exhibited by magnetoresistance measurements which showed increased ordering at the onset of 100 K and below. Although these samples showed ferromagnetic properties at room temperature, it seemed the magnetic ordering was not strong enough to display the PHE sinusoid at $T > 100$ K. This lack of strong ordering at higher temperatures is most likely due to the disruption by thermal agitations.

In CuO, PHE was observed with a positive dρ from room temperature to 5 K. This was discussed as being due to the p-type conductivity within this semiconductor. The maximum in dρ was observed at 100 K, which coincided with a visible resistivity minimum. The R vs. T in CuO showed characteristics of the Kondo effect with a resistivity minimum at 100 K and saturation in resistivity at the lowest temperatures (< 34 K). It was interesting to note that dρ diminished to a minimum at those low temperatures and became constant. The observation of a negative PHE in ZnO and a positive PHE in CuO led to the conclusion that the sign of PHE may be a way to tell what role the majority carriers in a material play in the magnetotransport properties at different temperatures. It was discussed that dρ was negative in semiconducting Ga(Mn)As [20] in contrast to ferromagnetic metals, where dρ is usually positive. This may be due to the way that electrons and holes contribute differently to spin–orbit coupling in ferromagnetic materials. Future studies could look at how the sign of dρ varies between different materials; this could in turn help to elucidate how electrons or holes contribute to the magnetization and magnetotransport properties of magnetic conductors.

From these results, it was clearly seen that undoped defect engineering metal/transition metal oxides are a rich material system for studying spin-dependent charge transport. Doping with additional impurities could add complexity to the properties of these materials. Further studies in both n- and p-type semiconductors can eventually lead to the observation of PHE at room temperature within a material that has strong magnetic properties at room temperature. This could then pave the way towards the development of sensor devices that utilize the PHE as their operating mechanism.

Acknowledgements Part of this research was supported by the National Science Foundation and the Army Research Office. We gratefully acknowledge the support from the Extreme Light Sources DARPA project W31P4Q-08-1-0003 administered by the University of Florida. The corresponding author would like to thank John Christopher Ledford for his assistance with measurements using the SQUID and PPMS facility in the Department of Materials Science and Engineering at North Carolina State University.

References

1. G.A. Prinz, Science **282**, 1660–1663 (1998)
2. S.A. Wolf, D.D. Awschalom, R.A. Buhrman, J.M. Daughton, S. von Molnár, M.L. Roukes, A.Y. Chtchelkanova, D.M. Treger, Science **294**, 1488–1495 (2001)
3. I. Žutić, J. Fabian, S. Das Sarma, Rev. Mod. Phys., **76**, 323–410 (2004)
4. H. Ohno, Science **281**, 951–956 (1998)
5. V. Avrutin, N. Isyumskaya, U. Ozgur, D.J. Silversmith, H. Morkoc, Proceedings IEEE **98**, 1288–1301 (2010)
6. V. Ström, B.J. Jönsson, K.V. Rao, E.D. Dahlberg, J. Appl. Phys. **81**, 5003–5005 (1997)
7. B.H. Miller, E.D. Dahlberg, Appl. Phys. Lett. **69**, 3932–3934 (1996)
8. D. Venus, F. Hunte, Phys. Rev. B **72**, 024404 (2005)
9. D. Venus, F. Hunte, E. Dahlberg, J. Magn. Magn. Mater., **286**, 191–195 (2005)
10. D. Venus, F. Hunte, I.N. Krivorotov, T. Gredig, E.D. Dahlberg, J. Appl. Phys. **93**, 8609–8611 (2003)
11. F. Hunte, *Determination of Exchange Anisotropy by ac-AMR and Planar Hall Effect*. PhD Dissertation, School of Physics and Astronomy, University of Minnesota, Twin Cities, MN, 2004
12. N.A. Spaldin, *Magnetic materials: fundamentals and applications*, 2nd edn. (Cambridge University Press, Cambridge, New York, 2011)
13. Y. Bason, L. Klein, J.B. Yau, X. Hong, C.H. Ahn, Appl. Phys. Lett. **84**, 2593–2595 (2004)
14. C.M. Hurd, *The Hall effect in metals and alloys* (Plenum Press, New York, 1972)
15. R.R. Birss, *Symmetry and magnetism* (North-Holland, Amsterdam, 1966)
16. P. Ciureanu, *Magnetoresistive sensors*, 1st edn. (Institute of Physics Publishing, Bristol, 1992)
17. T. McGuire, R. Potter, IEEE Trans. Magn. **11**, 1018–1038 (1975)
18. L. Guohong, Y. Tao, H. Qiang, Appl. Phys. Lett. **77**, 1032–1034 (2000)
19. A.O. Adeyeye, M.T. Win, T.A. Tan, G.S. Chong, V. Ng, T.S. Low, Sens. Actuators, A **116**, 95–102 (2004)
20. H.X. Tang, R.K. Kawakami, D.D. Awschalom, M.L. Roukes, Phys. Rev. Lett. **90**, 107201 (2003)
21. R. Arnab, P.S.A. Kumar, J. Phys. D Appl. Phys. **43**, 365001 (2010)
22. A. Schuhl, F.N. Van Dau, J.R. Childress, Appl. Phys. Lett. **66**, 2751–2753 (1995)
23. A.V. Trukhanov, S.V. Trukhanov, V.G. Kostishyn, L.V. Panina, V.V. Korovushkin, V.A. Turchenko, D.A. Vinnik, E.S. Yakovenko, V.V. Zagorodnii, V.L. Launetz, V.V. Oliynyk, T.I. Zubar, D.I. Tishkevich, E.L. Trukhanova, J. Magn. Magn. Mater. **462**, 127–135 (2018)
24. S.V. Trukhanov, A.V. Trukhanov, L.V. Panina, V.G. Kostishyn, V.A. Turchenko, E.L. Trukhanova, A.V. Trukhanov, T.I. Zubar, V.M. Ivanov, D.I. Tishkevich, D.A. Vinnik, S.A. Gudkova, D.S. Klygach, M.G. Vakhitov, P. Thakur, A. Thakur, Y. Yang, J. Magn. Magn. Mater. **466**, 393–405 (2018)
25. S.V. Trukhanov, N.V. Kasper, I.O. Troyanchuk, M. Tovar, H. Szymczak, K. Bärner, J. Solid State Chem. **169**, 85–95 (2002)
26. S.V. Trukhanov, L.S. Lobanovski, M.V. Bushinsky, V.A. Khomchenko, N.V. Pushkarev, I.O. Troyanchuk, A. Maignan, D. Flahaut, H. Szymczak, R. Szymczak, Eur. Phys. J. B Condens. Matter Complex Syst. **42**, 51–61 (2004)
27. S.V. Trukhanov, A.V. Trukhanov, A.N. Vasiliev, A.M. Balagurov, H. Szymczak, J. Exp. Theor. Phys. **113**, 819–825 (2011)
28. J.G. Reynolds, C.L. Reynolds, A. Mohanta, J.F. Muth, J.E. Rowe, H.O. Everitt, D.E. Aspnes, Appl. Phys. Lett. **102**, 152114 (2013)
29. R.E. Hummel, *Electronic properties of materials*, 3rd edn. (Springer, New York, 2005)
30. W.C. Mackrodt, R.F. Stewart, J.C. Campbell, I.H. Hillier, J. Phys. Colloques, **41**, C6-64-C66-67 (1980)
31. S. Mal, S. Nori, J. Chunming, J. Narayan, S. Nellutla, A.I. Smirnov, J.T. Prater, J. Appl. Phys. **108**, 073510 (2010)
32. S. Mal, J. Narayan, S. Nori, J.T. Prater, D. Kumar, Solid State Commun. **150**, 1660–1664 (2010)
33. J.M.D. Coey, Solid State Sci. **7**, 660–667 (2005)
34. R.J.D. Tilley, *Defects in solids* (Wiley, Hoboken, 2008)
35. G. Pacchioni, Chem. Phys. Chem **4**, 1041–1047 (2003)
36. J. Li, Y. Jiang, Y. Li, D. Yang, Y. Xu, M. Yan, Appl. Phys. Lett. **102**, 072404–072406 (2013)
37. T. Risse, A. Gonchar, T. Risse, H.-J. Freund, E. Giamello, Phys. Chem. Chem. Phys. **12**, 12520–12524 (2010)
38. J.H. Schulman, W.D. Compton, *Color centers in solids* (Pergamon Press, Oxford, 1963)
39. D. Gao, D. Gao, J. Zhang, G. Yang, J. Qi, M. Si, D. Xue, J. Phys. Chem. C **115**, 16405–16410 (2011)
40. B. Choudhury, A. Choudhury, Curr. Appl. Phys. **13**, 1025–1031 (2013)
41. Y.-C. Chen, E. Goering, L. Jeurgens, Z. Wang, F. Phillipp, J. Baier, T. Tietze, G. Schütz, Appl. Phys. Lett. **103**, 162405 (2013)
42. H. Ren, G. Xiang, G. Gu, X. Zhang, W. Wang, P. Zhang, B. Wang, X. Cao, J. Nanomater. **2012**, 295358 (2012)
43. S. Mal, T.-H. Yang, C. Jin, S. Nori, J. Narayan, J.T. Prater, Scripta Mater. **65**, 1061–1064 (2011)
44. D.F. Wang, J.M. Kim, V.T.T. Thuy, M.S. Seo, Y.P. Lee, J. Korean Phys. Soc. **58**, 1304–1306 (2011)
45. G. Xing, D. Wang, J. Yi, L. Yang, M. Gao, M. He, J. Yang, J. Ding, T.C. Sum, T. Wu, Appl. Phys. Lett. **96**, 112511 (2010)
46. G.D. Mahan, *Many-particle physics*, 3rd edn. (Kluwer Academic/Plenum Publishers, New York, 2000)
47. C. Kittel, *Introduction to solid-state physics*, 6th edn. (Wiley, New York, 1986)
48. J.D. Patterson, B.C. Bailey, *Solid-state physics: introduction to the theory*, 2nd edn. (Springer, Berlin, 2010)
49. J. Ghijsen, L.H. Tjeng, J. van Elp, H. Eskes, J. Westerink, G.A. Sawatzky, M.T. Czyzyk, Phys. Rev. B **38**, 11322–11330 (1988)
50. T. Kataoka, Y. Yamazaki, V.R. Singh, A. Fujimori, F.H. Chang, H.J. Lin, D.J. Huang, C.T. Chen, G.Z. Xing, J.W. Seo, C. Panagopoulos, T. Wu, Phys. Rev. B **84**, 153203 (2011)
51. T. Dietl, H. Ohno, F. Matsukura, J. Cibert, D. Ferrand, Science **287**, 1019 (2000)